ACS APPLIED MATERIALS & INTERFACES

Research Article

Cite This: ACS Appl. Mater. Interfaces 2017, 9, 44617−44624

www.acsami.org

Facile Electrochemical Synthesis of 2D Monolayers for High-Performance Thin-Film Transistors

Daniel S. Schulman,[†] Amritanand Sebastian,[‡] Drew Buzzell,[‡] Yu-Ting Huang,[§] Andrew J. Arnold,[∥] and Saptarshi Das*[,‡]

[†]Materials Science and Engineering, [‡]Engineering Science and Mechanics, and [∥]Electrical Engineering, Pennsylvania State University, University Park, Pennsylvania 16802, United States

[§]Department of Mechanical Engineering, University of Hong Kong, Pokfulam, Hong Kong

Supporting Information

ABSTRACT: In this paper, we report high-performance monolayer thin-film transistors (TFTs) based on a variety of two-dimensional layered semiconductors such as MoS_2, WS_2, and $MoSe_2$ which were obtained from their corresponding bulk counterparts via an anomalous but high-yield and low-cost electrochemical corrosion process, also referred to as electro-ablation (EA), at room temperature. These monolayer TFTs demonstrated current ON−OFF ratios in excess of 10^7 along with ON currents of 120 μA/μm for MoS_2, 40 μA/μm for WS_2, and 40 μA/μm for $MoSe_2$ which clearly outperform the existing TFT technologies. We found that these monolayers have larger Schottky barriers for electron injection compared to their multilayer counterparts, which is partially compensated by their superior electrostatics and ultra-thin tunnel barriers. We observed an Anderson type semiconductor-to-metal transition in these monolayers and also discussed possible scattering mechanisms that manifest in the temperature dependence of the electron mobility. Finally, our study suggests superior chemical stability and electronic integrity of monolayers even after being exposed to extreme electro-oxidation and corrosion processes which is promising for the implementation of such TFTs in harsh environment sensing. Overall, the EA process proves to be a facile synthesis route offering higher monolayer yields than mechanical exfoliation and lower cost and complexity than chemical vapor deposition methods.

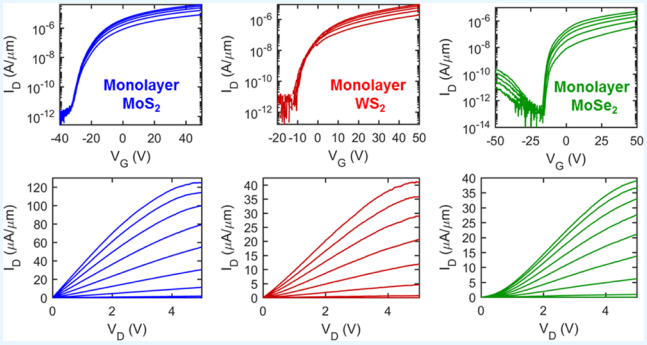

KEYWORDS: *electro-ablation, thin-film transistor, transition metal dichalcogenide, monolayers, electro-oxidation*

INTRODUCTION

The class of two-dimensional (2D) layered transition metal dichalcogenide (TMD) materials has garnered significant interest because of their robust semiconducting and optoelectronic properties down to the single monolayer limit. Monolayer MoS_2 field-effect transistors (FETs) have demonstrated low-temperature mobility values in excess of 1000 cm^2/V s. At room temperature, mobility values are ∼100 cm^2/V s and are predicted to increase to ∼480 cm^2/V s when encapsulated with high k materials that quench the homopolar phonon scattering.[1−3] Early on, semiconducting 2D materials such as MoS_2 were recognized for their ultrathin structure, ∼0.65 nm for a single monolayer, as a suitable replacement for the current high-performance Si technology. Note that the superior electrostatics offered by atomically thin monolayers reduce short-channel effects compared to multigated Si-based FETs.[4,5] Recently, highly scaled devices with gate lengths <10 nm have been demonstrated,[6,7] improvements in contact resistance have neared what is outlined by the ITRS roadmap,[6,8] and basic circuits such as logic inverters and signal amplifiers have been demonstrated.[9,10] Even if TMDs do not displace Si, their performance far exceeds that of current amorphous Si, amorphous oxide, and organic thin-film transistor (TFT) materials used in organic light-emitting diode and liquid crystal display panels.[11−13] Further, 2D materials provide a unique platform for various beyond-Boltzmann, ultra-low-power device concepts based on novel physical phenomena such as strain-induced semiconductor-to-metal transition (SMT),[14] exciton-mediated phase transition,[15,16] and quantum mechanical tunneling through atomically sharp 2D/2D interfaces.[17−20] Various non-von Neumann computing paradigms including neuromorphic and stochastic devices are also being explored based on TMDs.[21,22]

In the monolayer form, the TMDs are multivalley direct band gap semiconductors with strong spin-orbit coupling.[23,24] In contrast to indirect band gap multilayer TMDs, monolayers are well-suited toward optoelectronics such as photodetectors in which a single monolayer absorbs >5% incident sunlight,

Received: September 27, 2017
Accepted: December 6, 2017
Published: December 6, 2017

DOI: 10.1021/acsami.7b14711
ACS Appl. Mater. Interfaces 2017, 9, 44617−44624

light-emitting diodes with a strain tunable optical band gap, and optic modulators.[25−29] Given that they exhibit spin hall and valley hall effects, they are of particular interest for valleytronic and spintronic applications.[24,30] Despite the high demand for monolayer TMD materials, they have been either costly or challenging to acquire, hence the need for facile synthesis techniques such as the electro-ablation (EA) process for semiconductor grade MoS_2, WS_2, and $MoSe_2$ monolayers presented here.

The EA process[31] has key advantages over mechanical exfoliation and chemical vapor deposition (CVD) methods. Mechanical exfoliation results in extremely small, low yields of monolayers, requiring careful surface preparation and heating[32] or techniques such as gold-mediated exfoliation[33] to improve yields, whereas wafer-scale CVD growth of high-quality monolayers demands expensive infrastructure and resources in terms of higher processing temperatures and longer processing times. Although the EA process does not aim to compete with CVD growth,[34] it enables an alternative route for rapid, low-cost, high-yield, and room-temperature synthesis and access to a diverse set of 2D monolayers. In fact, the EA process could be complementary to the CVD processes because it can be used to planarizing CVD-grown multilayer TMDs into their corresponding monolayers. Additionally, the EA process points toward the superior chemical stability and electronic integrity of 2D monolayers when subjected to extreme electro-oxidation and corrosion environments. Such monolayer stability is attributed to a chemically inert basal plane, which is inherent to 2D materials, coupled with suppressed edge reactivity at the monolayer limit through the monolayer/substrate interaction.[31] Therefore, electronic sensors which require stability in chemically corrosive and strongly oxidizing environments can be implemented based on these TMD monolayers and will ultimately find their application in industries such as oil refining and polymer processing, automotive and aerospace, mining, and power generation. TMD-based sensors operating via a change in either electrical characteristics[35−37] or optical response[38] are capable of detecting environmental pollutants such as NH_3, NO_2, and H_2. Biocompatible MoS_2 FET devices have even been demonstrated for applications such as biomolecules, proteins, and pH sensing.[39−42]

EXPERIMENTAL PROCEDURE

The EA process to convert MoS_2, WS_2, and $MoSe_2$ multilayer films to monolayers originally reported by Das et al.[31] is schematically shown in Figure 1a−c. First, the TMD material is mechanically exfoliated onto a conductive 100 nm TiN film on Si. The lateral size of the exfoliated flake will ultimately determine the size of the subsequent monolayer, and hence high yields of monolayers with lateral dimensions of 10s of μm are easily achievable. The sample is then placed in a three-terminal electrochemical cell where the conductive TiN functions as the working electrode. Next, a relatively small anodic potential of less than ~1.4 V applied against an Ag/AgCl reference electrode for a period of time up to 120 s converts the exfoliated multilayers into their corresponding monolayers via an anomalous but self-limiting corrosion process consistently over the entire substrate irrespective of the initial thickness of the multilayer flakes. In particular, we used a 1 M LiCl solution as the electrolyte, although most cations and anions work, with a pH value of 2, 5, and 3 respectively, for MoS_2, WS_2, and $MoSe_2$. The EA process was carried out at anodic potentials of 1.4, 1.4, and 1.2 V versus Ag/AgCl for 120, 120, and 5 s for MoS_2, WS_2, and $MoSe_2$, respectively. The EA process parameters used in our study are tabulated in Figure 1j. Note that these parameters were used for the fabrication of TFTs based on these monolayers. These parameters were optimized independently for each

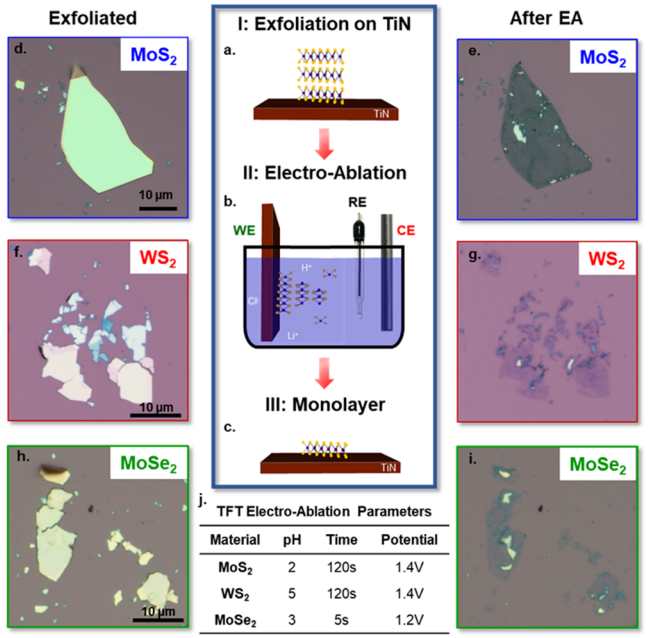

Figure 1. Schematic of the EA process (a) flakes of TMD are mechanically exfoliated onto a 100 nm thick conductive TiN film on Si. (b) Sample is placed into an electrochemical cell with a 1 M conductive LiCl electrolyte where an anodic potential is applied to TiN. (c) Within seconds, the bulk material begins to ablate into the solution converting the multilayer flakes to single monolayers strongly adhered to the TiN substrate. Optical images of (d,e) MoS_2, (f,g) WS_2, and (h,i) $MoSe_2$ after exfoliation and after EA. (j) Table for MoS_2, WS_2, and $MoSe_2$ showing the EA process parameters used for fabrication of TFTs.

material with the time chosen as to fully ablate the flake without over-etching to avoid any excessive defects in the monolayer. The anodic potentials used correspond to a small, ~0.1 V, overpotential, from what is required for the EA process to occur. The pH is particularly important for $MoSe_2$, as it determines bulk and monolayer ablation rates, corrosion profile, and ultimate monolayer morphology.[43]

Monolayers synthesized on a TiN substrate were subsequently transferred onto a 100 nm thermal SiO_2 on a p^{++} Si substrate for further characterization using a wet transfer process shown schematically in Figure 2.[44] A spin-casted polymethyl-methacrylate (PMMA) film is used to transfer the monolayers off the TiN substrate. The PMMA film, along with the monolayers, is detached from the TiN by submersing in 1 M NaOH at 90 °C, as shown in Figure 2c. This process differs from existing wet transfer processes[45] in that the TiN substrate is not sacrificially etched. Capillary action draws the NaOH solution to the PMMA/TiN interface, separating the hydrophobic PMMA/encapsulated-TMD from the hydrophilic substrate.[46] The detached film floats on the surface, which is then rinsed in deionized water three times and is finally transferred to the 100 nm thermal SiO_2/p^{++}-Si substrate. After baking at 50 °C for 10 min followed by 70 °C for 10 min, PMMA is removed with acetone, followed by rinsing with isopropyl alcohol. For transistor characterization, electron beam lithography was used to pattern the contact regions followed by electron beam evaporation of Ni/Au contacts.

RESULTS AND DISCUSSION

Figure 1d,f,h shows optical images of exfoliated MoS_2, WS_2, and $MoSe_2$ flakes with thicknesses on the order of 100s of nm before the EA process. Within seconds, the bulk layers begin to undergo an electro-oxidation process and are ablated into the solution, initiating at the edge, progressing inward (see Figure S1 for temporal AFM). The underlying monolayers remain

DOI: 10.1021/acsami.7b14711
ACS Appl. Mater. Interfaces 2017, 9, 44617−44624

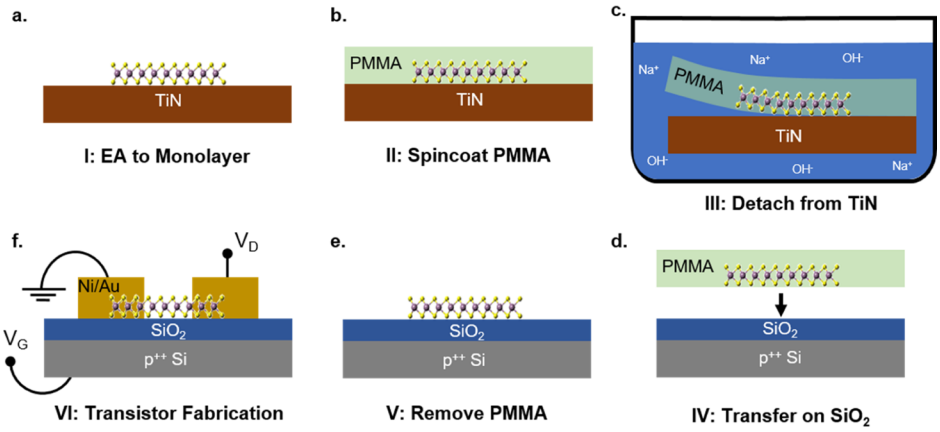

Figure 2. Schematic monolayer transfer and transistor fabrication. (a) EA converts TMDs to corresponding monolayers on the TiN substrate. (b) PMMA is then spun on the substrate. (c) Sample is submerged in 1 M NaOH until the PMMA film and monolayers detach from TiN. (d) PMMA film containing monolayer flakes is then transferred onto 100 nm SiO_2 on a p^{++} Si substrate. (e) PMMA is then removed using acetone/IPA. (f) Electron-beam lithography is used to pattern the contact regions followed by electron-beam evaporation of the Ni/Au contacts.

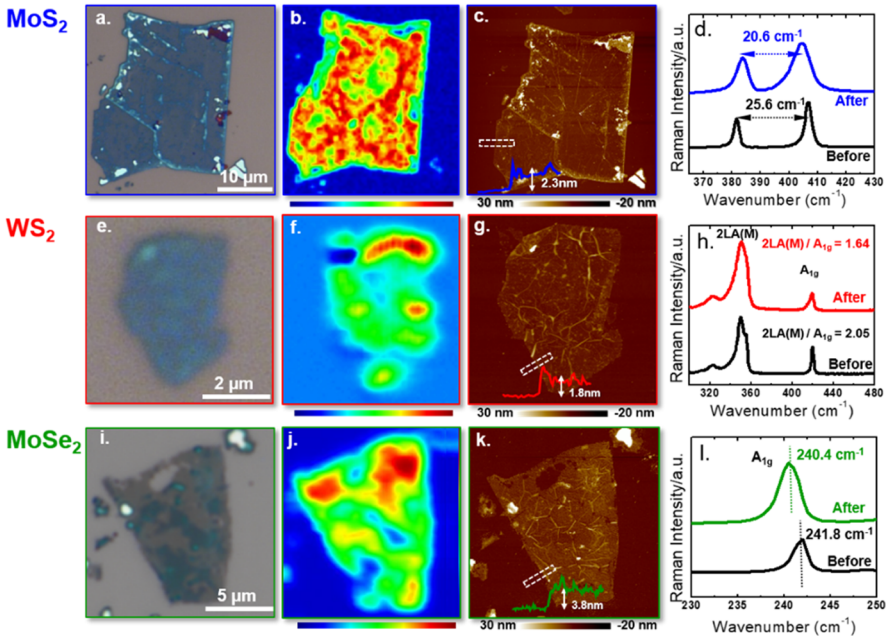

Figure 3. Characterization of electro-ablated MoS_2, WS_2, and $MoSe_2$ monolayers (a,e,i) optical images of MoS_2, WS_2, and $MoSe_2$ after transfer onto a 100 nm SiO_2 substrate. (b,f,j) PL intensity map showing intense PL across the monolayers at energies of ∼1.85, ∼1.95, and ∼1.55 eV corresponding to the direct band gaps of MoS_2, WS_2, and $MoSe_2$, respectively. The intensity is integrated from ±0.15 eV from the peak energy. (c,g,k) Atomic force microscope (AFM) images show a step height of ∼2.3, ∼1.8, and ∼3.8 nm for monolayer MoS_2, WS_2, and $MoSe_2$, respectively. (d,h,l) Raman spectra using a 532 nm laser on multilayer and monolayer MoS_2, WS_2, and $MoSe_2$, respectively. MoS_2 flakes show a decrease in the E_{2g} and A_{1g} peak separation from 25.6 to 20.6 cm^{-1} after conversion to monolayers. WS_2 flakes show a shift of the A_{1g} peak position from 420.7 to 419.2 cm^{-1}, with the 2LA(M) peak remaining at 350.5 cm^{-1}. The 2LA(M)/A_{1g} intensity ratio is reduced from 2.05 to 1.64. $MoSe_2$ shows a shift of the A_{1g} peak from 241.8 to 240.4 cm^{-1}. The $MoSe_2$ A_{1g} peak shifts from 241.8 to 240.4 cm^{-1}.

intact, strongly adhered to the substrate, as shown in Figure 1e,g,i for MoS_2, WS_2, and $MoSe_2$, respectively. Density functional theory (DFT) attributes the extraordinary monolayer stability to the strong binding energy between the bottom monolayer and the TiN substrate compared to the relatively weak interlayer binding energy.[31] Multilayer remnants are sometimes visible as islands toward the center of the monolayer regions owing to the incomplete corrosion process which is limited by the passivation of the TiN substrate. TiN catalyzes the production of oxidizing species such as O_2, H_2O_2, and so forth,[31,43] which is inhibited and ultimately rate-limited by the TiN oxidation during the EA process. Hence, there exists a competition between the bulk TMD ablation and substrate passivation dependent on the anodic potential, pH, and substrate.

The proposed reaction mechanism by Huang et al.[43] for electro-oxidation of TMDs with the general formula MX_2 is given by eq 1. The stability of MoO_3 (or WO_3) obtained as the reaction product depends on the pH. At the pH values used for each material, these products are hydrolyzed into aqueous species via eq 2. A more comprehensive study on the dependence of the EA process on the choice of the electrolyte, pH of the solution, applied anodic potential, and corrosion time is reported elsewhere for various 2D materials.[31,43]

DOI: 10.1021/acsami.7b14711
ACS Appl. Mater. Interfaces 2017, 9, 44617−44624

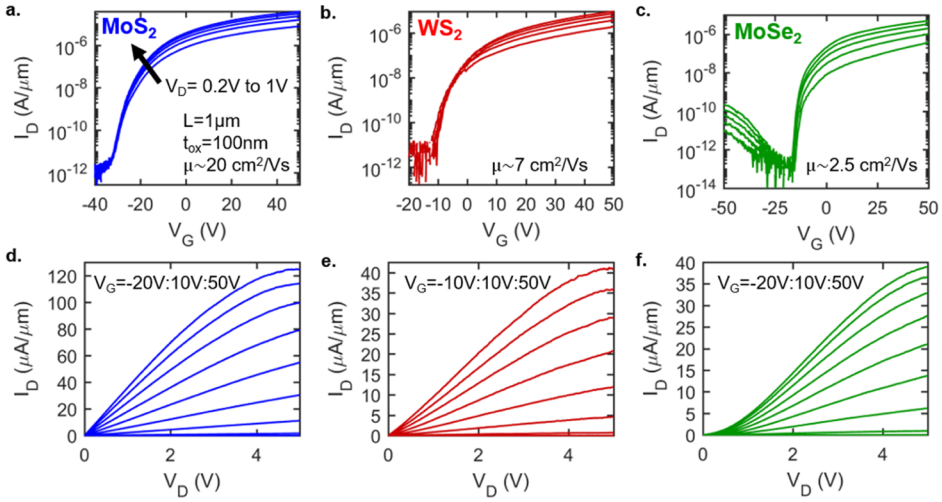

Figure 4. Monolayer TFTs. Transfer characteristics in the log scale at different drain biases (V_D) for backgated monolayer (a) MoS_2, (b) WS_2, and (c) $MoSe_2$ TFTs. All use a 100 nm thermal SiO_2 dielectric with Ni/Au contacts and a 1 μm channel length. The field-effect mobility values extracted from peak transconductance (g_m) were ~20, ~7, and ~2.5 cm^2/V s for MoS_2, WS_2, and $MoSe_2$, respectively. Output characteristics at different back gate voltages (V_G) for monolayer (d) MoS_2, (e) WS_2, and (f) $MoSe_2$. Ohmic-like linear current vs voltage characteristics are seen for MoS_2 and WS_2, whereas $MoSe_2$ displays SB-like sublinear current vs voltage characteristics.

$$MX_2 + H_2O/O_2 \rightarrow MO_3 + HXO_4^- \text{ or } XO_4^{2-} \quad (1)$$

$$MO_3 + 2OH^- \rightarrow MO_4^{2-} + H_2O \quad (2)$$

Photoluminescence (PL), atomic force microscopy (AFM), and Raman characterization of MoS_2, WS_2, and $MoSe_2$ electro-ablated flakes after transfer onto the SiO_2 substrate are shown in Figure 3. In general, the mechanical exfoliation process produces relatively large MoS_2 and $MoSe_2$ flakes, >10 μm, whereas the WS_2 flakes are much smaller, on the order of a few μm, as seen in Figure 3a,e,i. Intense PL shown in Figure 3b,f,j is observed across the entire monolayer MoS_2, WS_2, and $MoSe_2$ flakes at energies of ~1.85, ~1.95, and ~1.55 eV, corresponding to their monolayer direct band gaps, respectively.[47−49] The PL maps are of the integrated PL intensity from ±0.15 eV from the peak energy. It is believed that the spatial nonuniformity in the PL intensity is due to local defects interacting with gaseous species enhancing the PL.[50] Note that a dramatic increase in the PL yield occurs when the monolayer limit is reached for the TMDs owing to an abrupt indirect to direct band gap transition. The PL observed, thus, only exists in monolayer flakes which maintain their crystalline structure, providing strong evidence toward robustness of the electro-ablated monolayer TMDs.

AFM measured a step height of ~2.3, 1.8, and 3.8 nm for MoS_2, WS_2, and $MoSe_2$, respectively, as shown in Figure 3c,g,k. This is greater than the expected monolayer height of ~0.6 nm for MoS_2.[51] This discrepancy is hypothesized to arise from the incomplete hydrolyzation of the reaction products from equations 1 and 2. These undissolved oxide species would yield a greater than 0.6 nm step height, although the underlying crystalline semiconductor is still a single layer as supported by the PL and Raman spectroscopy. It should be noted that this is less than the ~4.5 nm step height measured when the material is still on the TiN substrate (see Figure S1). The wet transfer process may introduce contaminants at the TMD SiO_2 interface which could also result in a larger measured step height.

The MoS_2 Raman spectra from a multilayer flake and an electro-ablated monolayer are shown in Figure 3d. A reduction in the E_{2g} and A_{1g} peak separation from 25.6 to 20.6 cm^{-1} indicates a bulk-to-monolayer transition.[52] Similarly, WS_2 shows softening of the A_{1g} mode from 420.7 to 419.2 cm^{-1} with the 2LA peak remaining at 350.5 cm^{-1} as well as a reduction in the 2LA(M)/A_{1g} intensity ratio from 2.05 to 1.64 after conversion from a multilayer/bulk flake to the monolayer form,[52,53] as shown in Figure 3h. Figure 3l shows softening of the $MoSe_2$ A_{1g} mode from 241.8 to 240.4 cm^{-1}, confirming the transition from a multilayer to monolayer form.[49]

Monolayer MoS_2, WS_2, and $MoSe_2$ transistor characteristics are shown in Figure 4. The devices were measured under a vacuum of ~10^{-6} Torr to reduce hysteresis effects and threshold shifts due to ambient moisture.[54] MoS_2, WS_2, and $MoSe_2$ transfer characteristics shown in Figure 4a−c, respectively, exhibit minimal short-channel type effects such as drain-induced barrier lowering (DIBL). Although the relatively large 1 μm channel length and small geometric screening length, λ ~8 nm, calculated on the basis of $\lambda = \sqrt{t_{OX}t_B}$, where t_{OX} and t_B are, respectively, the thickness of the back gate oxide (100 nm) and thickness of the semiconducting channel (0.65 nm), predict that DIBL should not occur, Schottky barrier (SB) devices tend to exhibit other effects such as a strong drain voltage (V_D) dependence of the source SB width, known as drain-induced barrier thinning (DIBT), which produce DIBL-like characteristics.[55] Because monolayer devices have a small λ value, the DIBT or DIBL is on order of the measurement resolution, ~0.2 V. The small DIBL in the MoS_2 devices from V_D = 0.2 V to V_D = 0.4 V results from the forward-biased drain SB which is removed when the applied drain voltage is greater than the electron SB, that is, $V_D > \Phi_N$. Despite the electrostatics improvement offered by monolayers, the Ni work function pins relatively close to the conduction bands for MoS_2[56] and WS_2,[57] resulting in a hole injection SB sufficiently large to suppress any observable hole current. Calculations show that when approaching the monolayer limit of MoS_2, where the band gap increases from 1.2 to 1.8 eV,[48] the electron SB heights remain relatively similar, and hence, the hole SB increases substantially,[58] further suppressing any ambipolar behavior.

DOI: 10.1021/acsami.7b14711
ACS Appl. Mater. Interfaces 2017, 9, 44617−44624

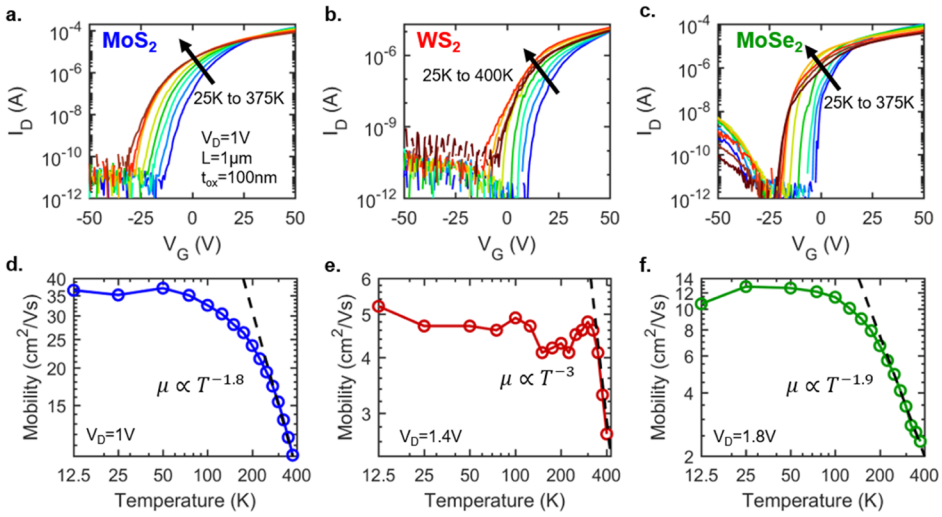

Figure 5. Temperature-dependent characterization of monolayer transistors. Log scale transfer characteristics of monolayer (a) MoS_2, (b) WS_2, and (c) $MoSe_2$ TFTs at V_D = 1 V from temperatures ranging from 25 to 400 K. Anderson-type semiconductor-to-metal transition is seen for all monolayer TFTs. (d) Field-effect mobility for MoS_2 at V_D = 1 V shows a $\mu \propto T^{-1.8}$ dependence from 12.5 to 375 K. (e) Field-effect mobility for WS_2 at V_D = 1.4 V shows a $\mu \propto T^{-3}$ dependence from 12.5 to 400 K. (f) Field-effect mobility for $MoSe_2$ at V_D = 1.8 V shows a $\mu \propto T^{-1.9}$ dependence from 12.5 to 400 K.

Although monolayer MoS_2 and WS_2 have relatively large band gaps of 1.85 and 1.95 eV, respectively, $MoSe_2$ has a smaller band gap of 1.55 eV.[47−49] Its smaller band gap, coupled with the fact that the Ni Fermi level pins further away from the conduction band edge when compared with MoS_2 and WS_2,[59] facilitates hole injection and hence the ambipolar characteristics seen in Figure 3c. The output characteristics for MoS_2, WS_2, and $MoSe_2$ in Figure 3d−f, respectively, points to a similar explanation. MoS_2 and WS_2 FETs show relatively linear "Ohmic type" output characteristics for small applied drain biases owing to a thinner and lower SB heights which ensures high tunneling probability for electron injection in the ON state of the device, whereas $MoSe_2$ FETs exhibit sublinear "Schottky type" output characteristics owing to a higher SB height for electron injection.

The field-effect mobility values of the devices were extracted at the location of peak transconductance, g_m (see Figures S2 and S3). MoS_2 devices with a 1 μm channel length have an average mobility of 19.4 ± 2.6 cm^2/V s for 7 devices and ON currents of ∼120 $\mu A/\mu m$ at a carrier density of ∼1.5 × 10^{13} cm^{-2}, which is comparable with the highest performing CVD monolayer materials.[35,60,61] The 11 WS_2 devices have a channel length of 500 nm as the flakes were much smaller and a mobility value of 6.7 ± 3.3 cm^2/V s, which is comparable to the highest performing CVD WS_2 materials.[62,63] Finally, $MoSe_2$ devices have a channel length of 1 μm and an average electron mobility of 2.6 ± 0.6 cm^2/V s for 9 devices, which is about an order of magnitude lower than what has been achieved with CVD materials.[64] For WS_2 and $MoSe_2$, although there are reports of higher mobility monolayer materials,[62−64] the ON currents reported here, namely, 40 $\mu A/\mu m$ for WS_2 and 40 $\mu A/\mu m$ for $MoSe_2$ at carrier densities of ∼10^{13} and ∼1.2 × 10^{13} cm^{-2}, respectively, are much larger.

Figure 5a−c shows the temperature-dependent transfer characteristics for MoS_2, WS_2, and $MoSe_2$ transistors, respectively. For all three materials, the absence of a temperature dependence of the subthreshold slope strongly suggests that at current levels above the gate leakage level of ∼10 pA, the devices are in the tunneling-dominated transport region, reinforcing the above discussion on the band alignment (see Figure S4 for additional measurements).[66] Although the interface trap capacitance can have a temperature dependence, it is unlikely that this would remove the temperature dependence of the thermionic regime. In the case of MoS_2, the primarily tunneling-dominated operation is not unexpected as the large monolayer band gap compared to the multilayer, 1.8 eV versus 1.2 eV,[48] permits a relatively large electron barrier while still maintaining a large enough hole barrier to suppress any ambipolar transport. In devices where the thermionic-to-tunneling transition current can be identified, the barrier height can be calculated using the Landauer transport model and the WKB approximation. Our device characteristics indicate that this transition occurs at a current level less than the leakage level of 10 pA for all monolayer TMDs reported here, that is, MoS_2, WS_2, and $MoSe_2$. As such, the SB height for electron injection must be greater than 0.5 eV, which is significantly higher than the previously reported multilayer values of 0.15 and 0.28 eV for MoS_2 and $MoSe_2$, respectively, with Ni contacts.[66]

The MoS_2 transfer characteristics shown in Figure 5a show an abrupt Anderson-type semiconductor/insulator-to-metal transition.[65] At low applied gate voltages where the carrier concentration is relatively low, the strongly bound electron system exhibits an "insulator" type behavior where the resistivity decreases, and hence current increases with increasing temperature. In the disordered 2D electron gas, an abrupt quantum phase transition to a "metallic" phase occurs when the energy exceeds the mobility edge or critical energy. The delocalized electrons, now stabilized by electron interactions, decrease in mobility with increasing temperature. This abrupt temperature-independent transition for MoS_2 occurs at V_G = 30 V which corresponds to a carrier density of ∼6 × 10^{12} cm^{-2}. For WS_2 shown in Figure 5b, this transition begins to occur at V_G = 50 V; however, the more positive threshold voltage for the WS_2 devices do not allow as high of a carrier concentration as in the MoS_2 devices. The transition for $MoSe_2$ also occurs but, unlike MoS_2, is not at the same V_G for all temperatures. This insulator-to-metal transition is desirable

DOI: 10.1021/acsami.7b14711
ACS Appl. Mater. Interfaces 2017, 9, 44617−44624

for high-power devices as it prevents thermal runaway from occurring.[67]

Figure 5d–f shows the temperature-dependent differential field-effect mobility for MoS_2, WS_2, and $MoSe_2$, respectively. The predictable temperature dependence on the mobility, and hence transconductance, of MoS_2 and $MoSe_2$ in particular makes them suitable as a temperature sensor with a wide range of ~25 to 400 K. The extracted mobility values are much lower than what is observed in bulk where the hall mobility of MoS_2 is ~100 cm^2/V s at 300 K and reaches a peak of ~300 cm^2/V s at 150 K. Bulk MoS_2 has a distinct low-temperature impurity scattering-limited regime and a high-temperature phonon scattering-limited regime with a $\mu \propto T^{-2.4}$ dependence.[68] This high-temperature phonon scattering, attributed to the zero-order homopolar mode, is quenched in single-layer MoS_2 devices, reducing to a predicted value of $\mu \propto T^{-1.69}$.[69] While this corresponds well with the extracted $T^{-1.8}$ for MoS_2 and for other reports in literature,[3,70] the predicted room temperature mobility is >400 cm^2/V s,[69] a full order of magnitude greater than what is observed here. This discrepancy indicates that the mobility is instead determined by extrinsic factors such as charged impurities in the SiO_2 and remote phonon scattering.[71] Ong and Fischetti show that at high temperatures, charged impurities dominate over phonons, and the temperature-dependent polarizability is a significant contributing factor to the mobility degradation and temperature dependence.[2] However, in the case of WS_2, the extracted high-temperature dependence of T^{-3} differs significantly from the $T^{-0.73}$ for mechanically exfoliated flakes[72] seen in literature, possibly arising from a less pristine interface for the electro-ablated monolayer. The $MoSe_2$ $T^{-1.9}$ dependence is relatively close to the reported values of $T^{-1.7}$ and $T^{-2.1}$ for few-layer $MoSe_2$.[73,74] Despite the clear presence of extrinsic mobility-affecting factors, little low-temperature mobility dependence is observed for MoS_2, WS_2, and $MoSe_2$, a signature of impurity-limited mobility. This low-temperature-independent behavior is also observed in the literature for MoS_2,[3] WS_2,[72] and $MoSe_2$.[73] These charged impurities, primarily in the SiO_2 substrate, result in an inhomogeneous localized charge distribution in the material which manifests itself in hopping-type transport and an increasing mobility with temperature.[71,75,76] Neither of these being observed in the ON state points to the impurities being relatively well-screened. A high k dielectric top gate would likely further screen the charged impurities and improve the mobility values as well.[1−3]

CONCLUSIONS

In summary, we have reported a facile, high-yield, room-temperature EA process for synthesizing a diverse set of TMD monolayers. The EA process points toward the extraordinary chemical stability of 2D materials in their monolayer form which are able to withstand extreme electro-oxidative conditions. The inert basal plane coupled with suppressed edge reactivity at the monolayer limit suggests that monolayer TMDs are suitable as the active component in harsh environmental sensors. EA synthesis has key advantages compared to mechanical exfoliation's low yields or the costly infrastructure associated with high-temperature CVD, providing an alternative, low-cost route for the synthesis of high-quality 2D monolayers. Monolayer TFTs synthesized via EA demonstrated ON−OFF ratios in excess of 10^7 along with ON currents of 120 $\mu A/\mu m$ for MoS_2, 40 $\mu A/\mu m$ for WS_2, and 40 $\mu A/\mu m$ for $MoSe_2$ which clearly outperform the existing TFT technologies. Various carrier transport phenomena were gleaned from temperature-dependent characterizations such as Anderson-type SMTs, the temperature dependence on electron mobility, and the observation that these monolayers have larger electron SBs than their multilayer counterparts which is partially compensated by their superior electrostatics and thin tunnel barriers. This work has demonstrated that EA synthesis can facilitate the study of the rich monolayer physics for a diverse set of materials, especially for those requiring inexpensive, high-yield, large domain materials.

ASSOCIATED CONTENT

Supporting Information

The Supporting Information is available free of charge on the ACS Publications website at DOI: 10.1021/acsami.7b14711.

Temporal dynamics of the electro-ablation process, monolayer transistor characterization statistics, temperature-dependent transistor characterization (PDF)

AUTHOR INFORMATION

Corresponding Author

*E-mail: sud70@psu.edu, das.sapt@gmail.com.

ORCID

Daniel S. Schulman: 0000-0002-0751-0578

Andrew J. Arnold: 0000-0002-9790-2128

Saptarshi Das: 0000-0002-0188-945X

Author Contributions

D.S.S. and S.D. conceived the experiments and analyzed the data. A.S., D.B., and Y.T.H. performed all the experiments related to electrochemistry and did the monolayer characterization after transferring onto SiO_2 substrate. D.S.S. and A.J.A. fabricated the thin-film transistors and performed all electrical measurements. The manuscript was written through contributions of all authors. All authors have given approval to the final version of the manuscript.

Notes

The authors declare no competing financial interest.

ACKNOWLEDGMENTS

The work of D.S.S. and S.D. was partially supported through grant no. ECCS-1640020 from National Science Foundation (NSF) and contract no. 2016-NE-2699 from Semiconductor Research Corporation. The work of A.S. and D.B. was partially supported through grant no. W911NF-17-1-0324 from Army Research Office (ARO). The work of A.J.A. was partially supported through grant no. FA9550-17-1-0018 from Air Force Office of Scientific Research (AFOSR) through the Young Investigator Program. The authors would like to thank Fu Zhang for assisting with the film transfer process. The authors would also like to acknowledge the technical staff members at the Material Research Institute at Penn State University.

REFERENCES

(1) Cui, X.; Lee, G.-H.; Kim, Y. D.; Arefe, G.; Huang, P. Y.; Lee, C.-H.; Chenet, D. A.; Zhang, X.; Wang, L.; Ye, F.; Pizzocchero, F.; Jessen, B. S.; Watanabe, K.; Taniguchi, T.; Muller, D. A.; Low, T.; Kim, P.; Hone, J. Multi-terminal transport measurements of MoS2 using a van der Waals heterostructure device platform. *Nat. Nanotechnol.* **2015**, *10*, 534−540.

(2) Ong, Z.-Y.; Fischetti, M. V. Mobility enhancement and temperature dependence in top-gated single-layer MoS2. *Phys. Rev. B: Condens. Matter Mater. Phys.* **2013**, *88*, 165316.

(3) Radisavljevic, B.; Kis, A. Mobility engineering and a metal−insulator transition in monolayer MoS2. *Nat. Mater.* **2013**, *12*, 815−820.
(4) Agarwal, T.; Yakimets, D.; Raghavan, P.; Radu, I.; Thean, A.; Heyns, M.; Dehaene, W. Benchmarking of MoS2FETs With Multigate Si-FET Options for 5 nm and Beyond. *IEEE Trans. Electron Devices* **2015**, *62*, 4051−4056.
(5) Ni, Z.; Ye, M.; Ma, J.; Wang, Y.; Quhe, R.; Zheng, J.; Dai, L.; Yu, D.; Shi, J.; Yang, J.; Watanabe, S.; Lu, J. Performance Upper Limit of sub-10 nm Monolayer MoS2Transistors. *Adv. Electron. Mater.* **2016**, *2*, 1600191.
(6) English, C. D.; Smithe, K. K. H.; Xu, R. L.; Pop, E. Approaching ballistic transport in monolayer MoS_2 transistors with self-aligned 10 nm top gates, *2016 IEEE International Electron Devices Meeting (IEDM)*, Dec 3−7, 2016; pp 5.6.1−5.6.4.
(7) Desai, S. B.; Madhvapathy, S. R.; Sachid, A. B.; Llinas, J. P.; Wang, Q.; Ahn, G. H.; Pitner, G.; Kim, M. J.; Bokor, J.; Hu, C.; Wong, H.-S. P.; Javey, A. MoS2 transistors with 1-nanometer gate lengths. *Science* **2016**, *354*, 99−102.
(8) Kappera, R.; Voiry, D.; Yalcin, S. E.; Branch, B.; Gupta, G.; Mohite, A. D.; Chhowalla, M. Phase-engineered low-resistance contacts for ultrathin MoS2 transistors. *Nat. Mater.* **2014**, *13*, 1128−1134.
(9) Wang, H.; Yu, L.; Lee, Y.-H.; Shi, Y.; Hsu, A.; Chin, M. L.; Li, L.-J.; Dubey, M.; Kong, J.; Palacios, T. Integrated circuits based on bilayer MoS2 transistors. *Nano Lett.* **2012**, *12*, 4674−4680.
(10) Cheng, R.; Jiang, S.; Chen, Y.; Liu, Y.; Weiss, N.; Cheng, H.-C.; Wu, H.; Huang, Y.; Duan, X. Few-layer molybdenum disulfide transistors and circuits for high-speed flexible electronics. *Nat. Commun.* **2014**, *5*, 5143.
(11) Nathan, A.; Kumar, A.; Sakariya, K.; Servati, P.; Sambandan, S.; Striakhilev, D. Amorphous silicon thin film transistor circuit integration for organic LED displays on glass and plastic. *IEEE J. Solid-State Circuits* **2004**, *39*, 1477−1486.
(12) Kamiya, T.; Nomura, K.; Hosono, H. Present status of amorphous In−Ga−Zn−O thin-film transistors. *Sci. Technol. Adv. Mater.* **2010**, *11*, 044305.
(13) Klauk, H. Organic thin-film transistors. *Chem. Soc. Rev.* **2010**, *39*, 2643−2666.
(14) Das, S. Two Dimensional Electrostrictive Field Effect Transistor (2D-EFET): A sub-60mV/decade Steep Slope Device with High ON current. *Sci. Rep.* **2016**, *6*, 34811.
(15) Zhu, B. R.; Chen, X.; Cui, X. D. Exciton Binding Energy of Monolayer WS2. *Sci. Rep.* **2015**, *5*, 9218.
(16) Fogler, M. M.; Butov, L. V.; Novoselov, K. S. High-temperature superfluidity with indirect excitons in van der Waals heterostructures. *Nat. Commun.* **2014**, *5*, 4555.
(17) Nguyen, L.-N.; Lan, Y.-W.; Chen, J.-H.; Chang, T.-R.; Zhong, Y.-L.; Jeng, H.-T.; Li, L.-J.; Chen, C.-D. Resonant tunneling through discrete quantum states in stacked atomic-layered MoS2. *Nano Lett.* **2014**, *14*, 2381−2386.
(18) Lam, K.-T.; Cao, X.; Guo, J. Device Performance of Heterojunction Tunneling Field-Effect Transistors Based on Transition Metal Dichalcogenide Monolayer. *IEEE Electron Device Lett.* **2013**, *34*, 1331−1333.
(19) Das, S.; Prakash, A.; Salazar, R.; Appenzeller, J. Toward low-power electronics: tunneling phenomena in transition metal dichalcogenides. *ACS Nano* **2014**, *8*, 1681−1689.
(20) Schulman, D. S.; Arnold, A. J.; Razavieh, A.; Nasr, J.; Das, S. The Prospect of Two-Dimensional Heterostructures: A review of recent breakthroughs. *IEEE Nanotechnol. Mag.* **2017**, *11*, 6−17.
(21) Arnold, A. J.; Razavieh, A.; Nasr, J. R.; Schulman, D. S.; Eichfeld, C. M.; Das, S. Mimicking Neurotransmitter Release in Chemical Synapses via Hysteresis Engineering in MoS2 Transistors. *ACS Nano* **2017**, *11*, 3110−3118.
(22) Cheng, P.; Sun, K.; Hu, Y. H. Memristive Behavior and Ideal Memristor of 1T Phase MoS2 Nanosheets. *Nano Lett.* **2016**, *16*, 572−576.
(23) Mak, K. F.; Lee, C.; Hone, J.; Shan, J.; Heinz, T. F. Atomically thin MoS2: a new direct-gap semiconductor. *Phys. Rev. Lett.* **2010**, *105*, 136805.
(24) Xiao, D.; Liu, G.-B.; Feng, W.; Xu, X.; Yao, W. Coupled spin and valley physics in monolayers of MoS2 and other group-VI dichalcogenides. *Phys. Rev. Lett.* **2012**, *108*, 196802.
(25) Ross, J. S.; Klement, P.; Jones, A. M.; Ghimire, N. J.; Yan, J.; Mandrus, D. G.; Taniguchi, T.; Watanabe, K.; Kitamura, K.; Yao, W.; Cobden, D. H.; Xu, X. Electrically tunable excitonic light-emitting diodes based on monolayer WSe2 p−n junctions. *Nat. Nanotechnol.* **2014**, *9*, 268−272.
(26) Baugher, B. W. H.; Churchill, H. O. H.; Yang, Y.; Jarillo-Herrero, P. Optoelectronic devices based on electrically tunable p−n diodes in a monolayer dichalcogenide. *Nat. Nanotechnol.* **2014**, *9*, 262−267.
(27) Withers, F.; Del Pozo-Zamudio, O.; Mishchenko, A.; Rooney, A. P.; Gholinia, A.; Watanabe, K.; Taniguchi, T.; Haigh, S. J.; Geim, A. K.; Tartakovskii, A. I.; Novoselov, K. S. Light-emitting diodes by band-structure engineering in van der Waals heterostructures. *Nat. Mater.* **2015**, *14*, 301−306.
(28) Bernardi, M.; Palummo, M.; Grossman, J. C. Extraordinary sunlight absorption and one nanometer thick photovoltaics using two-dimensional monolayer materials. *Nano Lett.* **2013**, *13*, 3664−3670.
(29) Castellanos-Gomez, A.; Roldán, R.; Cappelluti, E.; Buscema, M.; Guinea, F.; van der Zant, H. S. J.; Steele, G. A. Local strain engineering in atomically thin MoS2. *Nano Lett.* **2013**, *13*, 5361−5366.
(30) Zeng, H.; Dai, J.; Yao, W.; Xiao, D.; Cui, X. Valley polarization in MoS2 monolayers by optical pumping. *Nat. Nanotechnol.* **2012**, *7*, 490−493.
(31) Das, S.; Bera, M. K.; Tong, S.; Narayanan, B.; Kamath, G.; Mane, A.; Paulikas, A. P.; Antonio, M. R.; Sankaranarayanan, S. K. R. S.; Roelofs, A. K. A Self-Limiting Electro-Ablation Technique for the Top-Down Synthesis of Large-Area Monolayer Flakes of 2D Materials. *Sci. Rep.* **2016**, *6*, 28195.
(32) Huang, Y.; Sutter, E.; Shi, N. N.; Zheng, J.; Yang, T.; Englund, D.; Gao, H.-J.; Sutter, P. Reliable Exfoliation of Large-Area High-Quality Flakes of Graphene and Other Two-Dimensional Materials. *ACS Nano* **2015**, *9*, 10612−10620.
(33) Desai, S. B.; Madhvapathy, S. R.; Amani, M.; Kiriya, D.; Hettick, M.; Tosun, M.; Zhou, Y.; Dubey, M.; Ager, J. W., 3rd; Chrzan, D.; Javey, A. Gold-Mediated Exfoliation of Ultralarge Optoelectronically-Perfect Monolayers. *Adv. Mater.* **2016**, *28*, 4053−4058.
(34) Kang, K.; Xie, S.; Huang, L.; Han, Y.; Huang, P. Y.; Mak, K. F.; Kim, C. J.; Muller, D.; Park, J. High-mobility three-atom-thick semiconducting films with wafer-scale homogeneity. *Nature* **2015**, *520*, 656−660.
(35) Smithe, K. K. H.; English, C. D.; Suryavanshi, S. V.; Pop, E. Intrinsic electrical transport and performance projections of synthetic monolayer MoS2 devices. *2D Materials* **2016**, *4*, 011009.
(36) Liu, B.; Chen, L.; Liu, G.; Abbas, A. N.; Fathi, M.; Zhou, C. High-performance chemical sensing using Schottky-contacted chemical vapor deposition grown monolayer MoS2 transistors. *ACS Nano* **2014**, *8*, 5304−5314.
(37) Late, D. J.; Huang, Y.-K.; Liu, B.; Acharya, J.; Shirodkar, S. N.; Luo, J.; Yan, A.; Charles, D.; Waghmare, U. V.; Dravid, V. P.; Rao, C. N. R. Sensing behavior of atomically thin-layered MoS2 transistors. *ACS Nano* **2013**, *7*, 4879−4891.
(38) Feierabend, M.; Berghäuser, G.; Knorr, A.; Malic, E. Proposal for dark exciton based chemical sensors. *Nat. Commun.* **2017**, *8*, 14776.
(39) Sarkar, D.; Liu, W.; Xie, X.; Anselmo, A. C.; Mitragotri, S.; Banerjee, K. MoS2 field-effect transistor for next-generation label-free biosensors. *ACS Nano* **2014**, *8*, 3992−4003.
(40) Lee, J.; Dak, P.; Lee, Y.; Park, H.; Choi, W.; Alam, M. A.; Kim, S. Two-dimensional layered MoS2 biosensors enable highly sensitive detection of biomolecules. *Sci. Rep.* **2014**, *4*, 7352.
(41) Appel, J. H.; Li, D. O.; Podlevsky, J. D.; Debnath, A.; Green, A. A.; Wang, Q. H.; Chae, J. Low Cytotoxicity and Genotoxicity of Two-Dimensional MoS2 and WS2. *ACS Biomater. Sci. Eng.* **2016**, *2*, 361−367.

DOI: 10.1021/acsami.7b14711
ACS Appl. Mater. Interfaces 2017, 9, 44617−44624

(42) Chen, Y.; Tan, C.; Zhang, H.; Wang, L. Two-dimensional graphene analogues for biomedical applications. *Chem. Soc. Rev.* **2015**, *44*, 2681−2701.
(43) Huang, Y.-T.; Dodda, A.; Schulman, D. S.; Sebastian, A.; Zhang, F.; Buzzell, D.; Terrones, M.; Feng, S.-P.; Das, S. Anomalous Corrosion of Bulk Transition Metal Diselenides Leading to Stable Monolayers. *ACS Appl. Mater. Interfaces* **2017**, *9*, 39059−39068.
(44) Zhang, F.; Erb, C.; Runkle, L.; Zhang, X.; Alem, N. Etchant-free Transfer of 2D Nanostructures. *Nanotechnology* **2017**, DOI: 10.1088/1361-6528/aa9c21.
(45) Lee, Y.; Bae, S.; Jang, H.; Jang, S.; Zhu, S.-E.; Sim, S. H.; Song, Y. I.; Hong, B. H.; Ahn, J.-H. Wafer-scale synthesis and transfer of graphene films. *Nano Lett.* **2010**, *10*, 490−493.
(46) Schneider, G. F.; Calado, V. E.; Zandbergen, H.; Vandersypen, L. M. K.; Dekker, C. Wedging transfer of nanostructures. *Nano Lett.* **2010**, *10*, 1912−1916.
(47) Gutiérrez, H. R.; Perea-López, N.; Elías, A. L.; Berkdemir, A.; Wang, B.; Lv, R.; López-Urías, F.; Crespi, V. H.; Terrones, H.; Terrones, M. Extraordinary room-temperature photoluminescence in triangular WS2 monolayers. *Nano Lett.* **2013**, *13*, 3447−3454.
(48) Splendiani, A.; Sun, L.; Zhang, Y.; Li, T.; Kim, J.; Chim, C.-Y.; Galli, G.; Wang, F. Emerging photoluminescence in monolayer MoS2. *Nano Lett.* **2010**, *10*, 1271−1275.
(49) Tongay, S.; Zhou, J.; Ataca, C.; Lo, K.; Matthews, T. S.; Li, J.; Grossman, J. C.; Wu, J. Thermally driven crossover from indirect toward direct bandgap in 2D semiconductors: MoSe2 versus MoS2. *Nano Lett.* **2012**, *12*, 5576−5580.
(50) Tongay, S.; Suh, J.; Ataca, C.; Fan, W.; Luce, A.; Kang, J. S.; Liu, J.; Ko, C.; Raghunathanan, R.; Zhou, J.; Ogletree, F.; Li, J.; Grossman, J. C.; Wu, J. Defects activated photoluminescence in two-dimensional semiconductors: interplay between bound, charged and free excitons. *Sci. Rep.* **2013**, *3*, 2657.
(51) Frindt, R. F. Single Crystals of Mos2 Several Molecular Layers Thick. *J. Appl. Phys.* **1966**, *37*, 1928−1929.
(52) Terrones, H.; Del Corro, E.; Feng, S.; Poumirol, J. M.; Rhodes, D.; Smirnov, D.; Pradhan, N. R.; Lin, Z.; Nguyen, M. A. T.; Elías, A. L.; Mallouk, T. E.; Balicas, L.; Pimenta, M. A.; Terrones, M. New first order Raman-active modes in few layered transition metal dichalcogenides. *Sci. Rep.* **2014**, *4*, 4215.
(53) Zhao, W.; Ghorannevis, Z.; Amara, K. K.; Pang, J. R.; Toh, M.; Zhang, X.; Kloc, C.; Tan, P. H.; Eda, G. Lattice dynamics in mono- and few-layer sheets of WS2 and WSe2. *Nanoscale* **2013**, *5*, 9677−9683.
(54) Late, D. J.; Liu, B.; Matte, H. S. S. R.; Dravid, V. P.; Rao, C. N. R. Hysteresis in single-layer MoS2 field effect transistors. *ACS Nano* **2012**, *6*, 5635−5641.
(55) Jang, M.; Oh, J.; Maeng, S.; Cho, W.; Lee, S.; Kang, K.; Park, K. Characteristics of erbium-silicided n-type Schottky barrier tunnel transistors. *Appl. Phys. Lett.* **2003**, *83*, 2611−2613.
(56) Das, S.; Chen, H.-Y.; Penumatcha, A. V.; Appenzeller, J. High performance multilayer MoS2 transistors with scandium contacts. *Nano Lett.* **2013**, *13*, 100−105.
(57) Hwang, W. S.; Remskar, M.; Yan, R.; Protasenko, V.; Tahy, K.; Chae, S. D.; Zhao, P.; Konar, A.; Xing, H.; Seabaugh, A.; Jena, D. Transistors with chemically synthesized layered semiconductor WS2 exhibiting 105 room temperature modulation and ambipolar behavior. *Appl. Phys. Lett.* **2012**, *101*, 013107.
(58) Zhong, H.; Quhe, R.; Wang, Y.; Ni, Z.; Ye, M.; Song, Z.; Pan, Y.; Yang, J.; Yang, L.; Lei, M.; Shi, J.; Lu, J. Interfacial Properties of Monolayer and Bilayer MoS2 Contacts with Metals: Beyond the Energy Band Calculations. *Sci. Rep.* **2016**, *6*, 21786.
(59) Gong, C.; Zhang, H.; Wang, W.; Colombo, L.; Wallace, R. M.; Cho, K. Band alignment of two-dimensional transition metal dichalcogenides: Application in tunnel field effect transistors. *Appl. Phys. Lett.* **2013**, *103*, 053513.
(60) Chang, H.-Y.; Yogeesh, M. N.; Ghosh, R.; Rai, A.; Sanne, A.; Yang, S.; Lu, N.; Banerjee, S. K.; Akinwande, D. Large-Area Monolayer MoS2 for Flexible Low-Power RF Nanoelectronics in the GHz Regime. *Adv. Mater.* **2016**, *28*, 1818−1823.
(61) Schmidt, H.; Wang, S.; Chu, L.; Toh, M.; Kumar, R.; Zhao, W.; Neto, A. H. C.; Martin, J.; Adam, S.; Özyilmaz, B.; Eda, G. Transport properties of monolayer MoS2 grown by chemical vapor deposition. *Nano Lett.* **2014**, *14*, 1909−1913.
(62) Gong, Y.; Carozo, V.; Li, H.; Terrones, M.; Jackson, T. N. High flex cycle testing of CVD monolayer WS2 TFTs on thin flexible polyimide. *2D Materials* **2016**, *3*, 021008.
(63) Ovchinnikov, D.; Allain, A.; Huang, Y.-S.; Dumcenco, D.; Kis, A. Electrical Transport Properties of Single-Layer WS2. *ACS Nano* **2014**, *8*, 8174−8181.
(64) Wang, X.; Gong, Y.; Shi, G.; Chow, W. L.; Keyshar, K.; Ye, G.; Vajtai, R.; Lou, J.; Liu, Z.; Ringe, E.; Tay, B. K.; Ajayan, P. M. Chemical vapor deposition growth of crystalline monolayer MoSe2. *ACS Nano* **2014**, *8*, 5125−5131.
(65) Punnoose, A.; Finkel'stein, A. M. Metal-insulator transition in disordered two-dimensional electron systems. *Science* **2005**, *310* (5746), 289−291.
(66) Appenzeller, J.; Zhang, F.; Das, S.; Knoch, J. Transition Metal Dichalcogenide Schottky Barrier Transistors: A Device Analysis and Material Comparison. *2D Materials for Nanoelectronics*; CRC Press, 2016; pp 207−240.
(67) Wolpert, D.; Ampadu, P. *Managing Temperature Effects in Nanoscale Adaptive Systems*; Springer, 2012.
(68) Fivaz, R.; Mooser, E. Electron-Phonon Interaction in Semiconducting Layer Structures. *Phys. Rev.* **1964**, *136*, A833−A836.
(69) Kaasbjerg, K.; Thygesen, K. S.; Jacobsen, K. W. Phonon-limited mobility inn-type single-layer MoS2 from first principles. *Phys. Rev. B: Condens. Matter Mater. Phys.* **2012**, *85*, 115317.
(70) Fiori, G.; Szafranek, B. N.; Iannaccone, G.; Neumaier, D. Velocity saturation in few-layer MoS2 transistor. *Appl. Phys. Lett.* **2013**, *103*, 233509.
(71) Chen, J.-H.; Jang, C.; Xiao, S.; Ishigami, M.; Fuhrer, M. S. Intrinsic and extrinsic performance limits of graphene devices on SiO2. *Nat. Nanotechnol.* **2008**, *3*, 206−209.
(72) Ovchinnikov, D.; Allain, A.; Huang, Y.-S.; Dumcenco, D.; Kis, A. Electrical transport properties of single-layer WS2. *ACS Nano* **2014**, *8*, 8174−8181.
(73) Chamlagain, B.; Li, Q.; Ghimire, N. J.; Chuang, H.-J.; Perera, M. M.; Tu, H.; Xu, Y.; Pan, M.; Xaio, D.; Yan, J.; Mandrus, D.; Zhou, Z. Mobility improvement and temperature dependence in MoSe2 field-effect transistors on parylene-C substrate. *ACS Nano* **2014**, *8*, 5079−5088.
(74) Larentis, S.; Fallahazad, B.; Tutuc, E. Field-effect transistors and intrinsic mobility in ultra-thin MoSe2 layers. *Appl. Phys. Lett.* **2012**, *101*, 223104.
(75) Ghatak, S.; Pal, A. N.; Ghosh, A. Nature of electronic states in atomically thin MoS2 field-effect transistors. *ACS Nano* **2011**, *5*, 7707−7712.
(76) Chan, M. Y.; Komatsu, K.; Li, S.-L.; Xu, Y.; Darmawan, P.; Kuramochi, H.; Nakaharai, S.; Aparecido-Ferreira, A.; Watanabe, K.; Taniguchi, T.; Tsukagoshi, K. Suppression of thermally activated carrier transport in atomically thin MoS2 on crystalline hexagonal boron nitride substrates. *Nanoscale* **2013**, *5*, 9572−9576.

DOI: 10.1021/acsami.7b14711
ACS Appl. Mater. Interfaces 2017, 9, 44617−44624